J. Fluid Mech. (2009), *vol.* 641, *pp.* 51–61.
doi:10.1017/S0022112009992175

Obstructed shear flows: similarities across systems and scales

MARCO GHISALBERTI†

School of Environmental Systems Engineering, University of Western Australia, Crawley, WA 6009, Australia

(Received 29 April 2009; revised 9 September 2009; accepted 10 September 2009)

In this paper, I show that a range of environmental flows are inherently dynamically similar. These flows, which are partially obstructed by a permeable medium, are here termed 'obstructed shear flows'. Examples include aquatic flows over sediment beds, submerged vegetation canopies and coral reefs, as well as atmospheric flows over crop canopies, forests and cities ('urban canopies'). While the density and geometry of the obstructions may vary, the drag in each system generates a velocity profile with an inflection point. This renders the flow unstable. Consequently, it is expected that (*a*) the dominant interfacial turbulent structure in obstructed shear flows will be a Kelvin–Helmholtz-type vortex, and (*b*) that this instability will engender hydrodynamic similarities among obstructed shear flows. Such similarities have been hypothesized but not yet fully explored. An extensive review of existing data confirms these dynamic similarities on scales of O(mm) to O(10 m). The extent of shear penetration into the obstruction, which is a primary determinant of residence time in the obstruction, scales upon the drag length scale. Other relationships that link the strength of turbulence and the 'slip' velocity at the top of the obstruction to the friction velocity (u_*) are also evident. The relationships presented here provide predictive capability for flow and transport in obstructed shear flows and suggest the possibility of a single framework to describe such flows on all scales.

Key words: atmospheric flows, free shear layers, instability

1. Introduction

Flows over permeable media (here termed 'obstructed shear flows') are ubiquitous in the environment. Such permeable media include sediment beds, submerged vegetation canopies and coral reefs in the aquatic environment and crop canopies, forests and cities in the terrestrial environment. The physical, chemical and biological properties of the fluid within the permeable medium often differ greatly from those of the fluid outside it. It is therefore critical that we understand the rate at which momentum, mass and heat are exchanged between the two regions. In the study of such varied phenomena as pore water fluxes from sediments, the impact of forests on the global carbon cycle or the amelioration of water quality by submerged vegetation, our predictive capabilities are limited.

There is direct experimental evidence of Kelvin–Helmholtz-type vortices in flows over vegetation canopies (figure 1). This instability, commonly observed in density-stratified flows (Kundu & Cohen 2004) and regions where parallel streams merge

† Email address for correspondence: ghisalbe@sese.uwa.edu.au

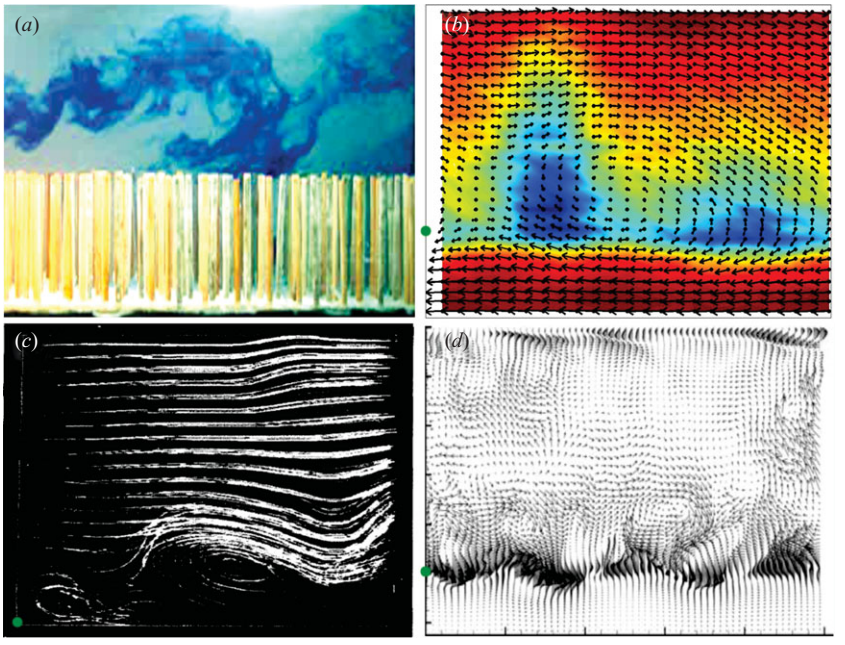

FIGURE 1. Evidence of Kelvin–Helmholtz-type vortices in obstructed shear flows. (*a*) The injection of blue food dye above rigid model vegetation (Ghisalberti & Nepf 2005, reproduced with the kind permission of Springer). (*b*) The phase-averaged velocity field (in the reference frame of the mean channel velocity) in a flow with rigid model vegetation (manuscript in preparation). (*c*) Image of particle streaks above a canopy of flexible model vegetation (Ikeda & Kanazawa 1996, reproduced with the kind permission of ASCE). (*d*) Instantaneous velocity perturbations in direct numerical simulation of flow above a packed bed ($n = 0.95$, Breugem, Boersma & Uittenbogaard 2006, reproduced with the kind permission of Cambridge University Press). In all cases, the flow is from left to right. In (*b*), (*c*) and (*d*), the location of the interface (i.e. the top of the obstruction) is indicated by a green dot. It is expected that mixing at the interface of all the permeable media discussed here is dominated by such vortical structures. Blue regions in (*b*) represent vertical momentum transport; the downward sweep at the front of the vortex is the dominant mechanism for mixing in the exchange zone.

(Chu & Babarutsi 1988), is generated by an inflection point in the mean velocity profile. In canopy flows, the vortices are responsible for the majority of vertical transport across the top of the canopy (Gao, Shaw & Paw U 1989; Finnigan 2000; Ghisalberti & Nepf 2009). The vortices engender strong similarity in the turbulent properties of canopy flows, as demonstrated by Raupach, Finnigan & Brunet (1996). For many other types of obstructed shear flow, the mean velocity profile is known to contain an inflection point; the inflection point is located roughly at the top of the obstruction (referred to hereafter as the 'interface'). Inflectional profiles in flows over a packed bed, a coral reef and an urban canopy are shown in figure 2. In the study of many such systems, however, there is little evidence of the existence and predominance of coherent interfacial vortices. A classical example is flow over sediment (i.e. packed) beds. Although mixing at the sediment–water interface is almost invariably regarded as occurring at molecular rates (Lorke *et al.* 2003), numerical simulations (figure 1*d*) reveal that the flow near a highly permeable packed bed is dominated by a Kelvin–Helmholtz-type instability (Breugem *et al.* 2006). The purpose of this paper is to highlight a consistency of hydrodynamic/aerodynamic behaviour in obstructed shear

System	Drag length scale, $(C_Da)^{-1}$	Height (h) required for $C_Dah > 0.1$
Sediment bed	O(1–10 mm)	O(0.1–1 mm)
Coral reef	O(10 cm)	O(1 cm)
Aquatic vegetation	O(10–100 cm)	O(1–10 cm)
Forest	O(10 m)	O(1 m)
Urban canopy	O(10–100 m)	O(1–10 m)

TABLE 1. Typical drag length scales of permeable media.

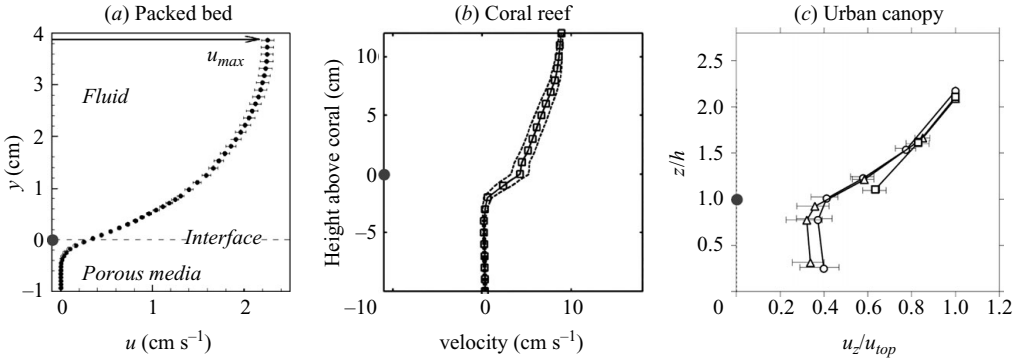

FIGURE 2. Inflectional velocity profiles in flows over three permeable media with differing length scales. (*a*) Oil flow over a packed bed of glass spheres ($n = 0.41$, $(C_Da)^{-1} \sim O$(1 cm), Goharzadeh, Khalili & Jørgensen 2005, reproduced with the kind permission of the American Institute of Physics) (*b*) Aquatic flow over a coral reef ($(C_Da)^{-1} \sim O$(10 cm), Reidenbach, Koseff & Koehl 2009, reproduced with the kind permission of ASLO) (*c*) Atmospheric flow over an urban canopy ($(C_Da)^{-1} \sim O$(10 m), Rotach *et al.* 2005, reproduced with the kind permission of Springer). In all cases, the inflection point (the point of maximum velocity gradient) and the interface (marked with a dot) are approximately coincident.

flows. In the absence of direct vortex visualization in many of these systems, the similarity of their dynamics (i.e. the physical signature of the vortices) will be demonstrated.

A permeable medium is characterized by its height (h) and its drag length scale, $(C_Da)^{-1}$. Here, C_D is the drag coefficient of the medium and a is the frontal area per unit volume, both averaged over the height of the medium. Typical drag length scales are provided in table 1. The drag length scale is a more accurate measure of the flow resistance within the obstruction than the porosity (n); the lower the drag length scale, the greater the resistance. As shown in figure 3, the drag exerted by the obstruction generates the unstable velocity profile. The ratio of the obstruction height to the drag length scale (i.e. C_Dah) must be greater than approximately 0.1 for obstructed shear flow behaviour to emerge (Nepf *et al.* 2007). If $C_Dah < 0.1$, the flow has the characteristics of a rough boundary layer, with no inflection point in the mean velocity profile. The vortices that result from the unstable profile grow downstream, reaching their equilibrium size a distance L_T from the front of the obstruction. This transition length scales upon the drag length scale (Ghisalberti & Nepf 2009). Relative to the fully developed flow, turbulent mixing in the region $x < L_T$ is diminished because of the reduced vortex scale but there can be strong vertical advective fluxes due to the deceleration of fluid within the obstruction. Flexible media

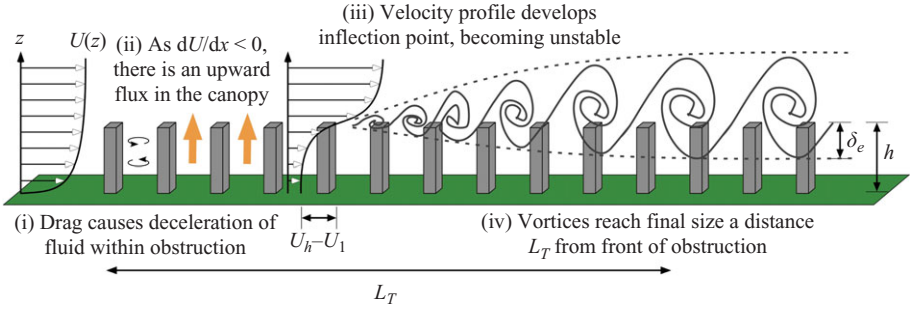

FIGURE 3. The evolution of flow along a submerged permeable medium. The distance required for full flow development L_T scales upon the drag length scale of the obstruction.

(particularly vegetation canopies) exhibit a low-frequency coherent waving due to vortex passage. The downward motion at the front of the vortex (figure 1*b*) creates a pocket of plant deflection that travels smoothly along the canopy (the 'waving wheat' phenomenon). Known as the *monami* in aquatic systems and the *honami* in terrestrial systems, this oscillation of the elements and the drag they exert can significantly diminish the residence time within the obstruction (Ghisalberti & Nepf 2009).

The dynamics of obstructed shear flows can be characterized by a few important velocity and length scales. The key length scale is δ_e, the penetration of the vortices (and the shear layer they define) into the obstruction (figure 3). This penetration is defined as extending from the interface ($z = h$, where the turbulent shear stress is maximized) to the point where the stress has decayed to 10 % of the interfacial value. The upper portion of the obstruction ($h - \delta_e < z < h$, termed the 'exchange zone') is flushed rapidly by the vortices, whereas the lower portion has reduced rates of mixing (Ghisalberti & Nepf 2005). The length scale δ_e is therefore a primary determinant of the mean residence time within the obstruction (Nepf *et al.* 2007). The important velocities are that at the interface (U_h) and that deep within the obstruction, where turbulent stresses are unimportant (U_1). Note that in studies of porous media, the product $U_1 n$ is typically termed the Darcy velocity. Finally, the friction velocity (u_*) is defined as the square root of the interfacial stress (normalized by fluid density).

1.1. *Objective*

To demonstrate the dynamic similarity amongst obstructed shear flows, four relationships between length and velocity scales are investigated here, as follows:

(*a*) The extent to which the length scale of the roughness $(C_D a)^{-1}$ determines the vertical transport length scale δ_e.

(*b*) The link between the shear stress (as indicated by u_*) and the 'slip' velocity at the interface ($= U_h - U_1$). In studies of dense porous media (DPM), this slip velocity is often taken to be zero, leading to underprediction of the interfacial flow speed.

(*c*) The relationship between u_* and the intensity of interfacial turbulence in the vertical direction (w_{rms}).

(*d*) The anisotropy of the turbulence, as indicated by the ratio of the vertical turbulence intensity at the interface (w_{rms}) to that in the streamwise direction (u_{rms}).

The purpose of this analysis is to show that all obstructed shear flows exhibit the same dynamic relationships. The first three relationships link a parameter that is

prescribed or known ($u_*, (C_D a)^{-1}$) to one that is unknown and directly relevant to the interfacial dynamics. The scaling coefficients in these three relationships provide predictive capability for flow and transport in obstructed shear flows. The fourth relationship examines the structure of the turbulence, which is expected to differ from that in a boundary layer.

2. Data extraction

Data were taken from flows over submerged aquatic vegetation canopies [in the laboratory, rigid (Dunn, Lopez & Garcia 1996; Nepf & Vivoni 2000; Ghisalberti & Nepf 2002; Poggi *et al.* 2004; Ghisalberti & Nepf 2004, 2006; Murphy, Ghisalberti & Nepf 2007) and waving (Ghisalberti & Nepf 2002, 2006)], terrestrial vegetation canopies [in the field (Shaw *et al.* 1974; Wilson *et al.* 1982; Baldocchi & Meyers 1988; Amiro 1990*a*,*b*; Gardiner 1994; Katul & Albertson 1998; Kruijt *et al.* 2000; Novak *et al.* 2000; Yi *et al.* 2005; Su *et al.* 2008) and laboratory (Seginer *et al.* 1976; Raupach, Coppin & Legg 1986; Brunet, Finnigan & Raupach 1994; Novak *et al.* 2000)], urban canopies [field (Oikawa & Meng 1995; Louka, Belcher & Harrison 2000; Rotach *et al.* 2005) and laboratory (Macdonald 2000; Cheng & Castro 2002; Kastner-Klein & Rotach 2004)], coral reefs [laboratory (Lowe, Koseff & Monismith 2005; Lowe 2005; Reidenbach, Koseff & Monismith 2007)], shallow flows horizontally adjacent to (rather than over) vegetation stands [laboratory (Pasche & Rouvé 1985; White & Nepf 2007)] and flows over DPM [laboratory (Gupte & Advani 1997; Goharzadeh *et al.* 2005; Agelinchaab, Tachie & Ruth 2006)]. The term 'dense porous medium' is used here to describe tightly packed obstructions ($(C_D a)^{-1} \lesssim 1$ cm) and includes packed granular beds, fibrous beds and rod arrays. In this study, these media are treated as an analogue of sediment beds in aquatic systems. The rigid aquatic vegetation data includes unpublished results from high-density arrays.

Some restrictions were placed upon the data used. Firstly, the obstruction had to be sufficiently dense (or tall) to generate an inflection point in the velocity profile. As discussed in § 1, this is true if $C_D a h > 0.1$. For real systems, this is not an overly restrictive condition (table 1). In the particular comparison of δ_e and $(C_D a)^{-1}$, the bed could not arrest vortex penetration. As the scaling coefficient in the relationship $\delta_e \sim (C_D a)^{-1}$ was expected to be roughly 0.25 in the absence of bed effects (Nepf *et al.* 2007), only obstructions with $C_D a h > 0.25$ were used in that comparison. Secondly, aquatic flows where the free surface had a dynamic impact were not considered. In shallow flows, the free surface can restrict vortex growth and strength (Nepf & Vivoni 2000). To first order, roughly two-thirds of the vortices exist above the canopy in vegetated flows (Ghisalberti & Nepf 2004). So, denoting the flow depth as H, only flows for which $C_D a(H - h) > 0.5$ were considered. Thirdly, flows with waving vegetation canopies were used in the third and fourth comparisons only, where definition of the obstruction height is not critical. Finally, flows with significant density stratification were not considered. Only atmospheric flows classified as 'near neutral' (for which $h/|L| \ll 1$, where L is the Monin–Obukhov length) were included. In all, data from 109 flows were used.

The parameters involved in the scaling of shear penetration into the obstruction (namely C_D, a and δ_e) can be difficult to estimate from the literature. Here, I lay out the method of estimating these three parameters when they were not explicitly provided; this is particularly tricky for DPM.

2.1. *Drag coefficient*

Measurements of C_D in an array of obstacles are surprisingly inconsistent. This is due partially to an inconsistency of definition; it is defined here as

$$C_D = \frac{F_D}{(\rho A_f U_c^2)/2}, \tag{2.1}$$

where F_D is the average drag force on an array element of frontal area A_f, ρ is the fluid density and U_c is a representative fluid velocity within the array. This inconsistency notwithstanding, the measured drag coefficients in the literature vary by more than an order of magnitude (0.3–3.7). This range is not explained by Reynolds number variations and can be attributed to three factors. Firstly, the impact of element wakes on the flow separation and drag of their downstream neighbours is complex and varies with Reynolds number and array density. Secondly, the frontal area of an individual element can be, particularly in forests, difficult to estimate. Finally, the 'representative' fluid velocity described above can be taken as U_h, U_1 or anything in between (compounding the uncertainty, this velocity is then squared in evaluation of C_D). The estimation of C_D is therefore not a trivial issue, and direct measurements are almost always required. For this work, if C_D was not measured directly, the average measured value for that system (approximately 0.5 for forests, 1 for aquatic vegetation, coral reefs and urban canopies) was assigned.

It is important to note that, strictly speaking, the drag length scale of an obstruction should incorporate the medium porosity (i.e. $n(C_D a)^{-1}$, Coceal & Belcher 2004). However, this correction is only significant for DPM, for which C_D is virtually impossible to predict (see § 2.4). Consequently, the simpler definition of the drag length scale is employed here.

2.2. *Frontal area*

The frontal area per unit volume (a) is easy to deduce for simple geometry (cylinders, spheres) but tricky for complex structures such as leafy trees. For forests, the frontal area was taken to be half the one-sided leaf area (following Raupach *et al.* 1996). In other words, if the leaf area index (LAI) is provided, then $a = \mathrm{LAI}/2h$. This 'halving' of the frontal area led to a doubling of any drag coefficients calculated using the one-sided leaf area. Urban canopy studies typically employ λ_f, a frontal area per unit ground area, such that $a = \lambda_f / h$. For a bed of spheres of diameter d, it can be shown that

$$a = \tfrac{3}{2}(1 - n)/d. \tag{2.2}$$

2.3. *Shear penetration*

In most cases, the shear penetration into the obstruction (δ_e) was taken as the distance over which the turbulent shear stress decays to 10 % of its maximum value (at the interface). In the absence of detailed stress profiles, δ_e was estimated from the profile of mean velocity. Specifically, assuming a flux-gradient relationship for momentum, it was taken as the distance over which the velocity gradient decays to 10 % of its interfacial value.

2.4. *Dense porous media*

In the case of DPM, the combination of dense packing and low Reynolds numbers make the estimation of C_D virtually impossible. Furthermore, the shear penetration into packed beds is typically of the order of the bed element diameter (Goharzadeh *et al.* 2005). The drag length scale ($(C_D a)^{-1}$) is a bulk parameter, defined over many

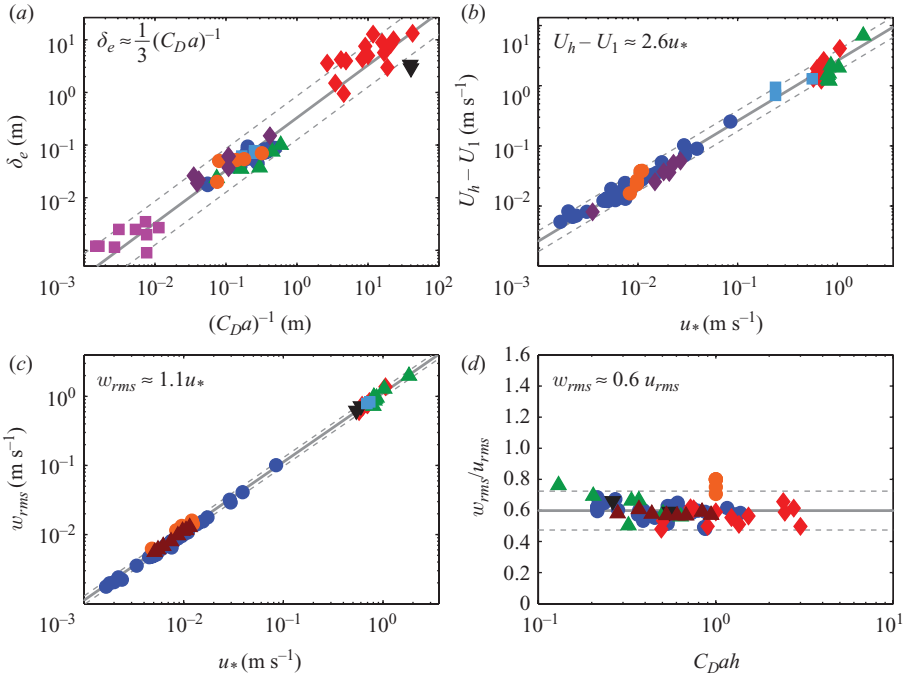

FIGURE 4. Four key dynamic relationships in obstructed shear flows. The data are taken from several systems: experimental flows over rigid model aquatic vegetation (●), waving model aquatic vegetation (▲), model terrestrial vegetation (▲), model urban canopies (■), coral reefs (●) and DPM (■), experimental flows horizontally adjacent to vegetation stands (♦) and real flows over terrestrial vegetation (♦) and urban canopies (▼). For each of the three relationships presented in (*a*), (*b*) and (*c*), $R^2 \geqslant 0.95$ in log space. The dashed lines represent the 90 % prediction interval.

inter-element spacings within the obstruction. Even for a perfectly packed bed, the resistance imparted on the flow will vary significantly over the scale of a single bed element. Thus, a true comparison of δ_e and $(C_D a)^{-1}$ is not possible for DPM. The comparison that can be made is that between δ_e and a^{-1}, where a nominal value of a is used for packed beds (namely, that in (2.2)). In effect, a drag coefficient of unity has been assumed for the purpose of drawing comparison amongst DPM. Importantly, however, the similarity of shear penetration behaviour between DPM and other obstructed shear flows cannot be examined.

3. Similarity of obstructed shear flows

The similarity of obstructed shear flows across the range of systems and scales (from $O(1\text{ mm})$ to $O(10\text{ m})$) is demonstrated in figure 4. In all four cases, there is a clear physical relationship that is effectively independent of the shape and configuration of the obstructions in the permeable medium. The collapse of the data provides strong evidence of similarity in the structure of the mean flow and turbulence among obstructed shear flows. Furthermore, it suggests that all obstructed shear flows can be analysed within a common framework.

Figure 4(*a*) shows that the drag length scale sets the vortex/shear penetration into the obstruction. As both C_D and a can (usually) be reasonably estimated *a priori*, the depth to which the obstruction is rapidly flushed can be predicted in the absence

of any measurements. In figure 4(*b*), the slip velocity is shown to scale upon the friction velocity. It is slightly counter-intuitive that the ratio $(U_h - U_1)/u_*$ is not a function of packing density; one might expect the slip velocity to be reduced in denser obstructions. However, a simple scaling argument confirms such a relationship. By definition of the Prandtl mixing length (l), $u_* = l(h) \times \partial U/\partial z(h)$. As the mixing length inside the canopy scales on δ_e (Ghisalberti & Nepf 2004), this becomes $u_* \sim \delta_e \times (U_h - U_1)/\delta_e = U_h - U_1$. In figures 4(*c*) and 4(*d*), the deviation of obstructed shear flows from boundary layers becomes evident. In particular, the vortices in obstructed shear flows generate vertical fluxes in excess of those in a boundary layer. The mean obstructed shear flow values of w_{rms}/u_* (1.09 ± 0.02, with 95 % confidence) and w_{rms}/u_{rms} (0.60 ± 0.04) are statistically distinct from the values in the logarithmic region of a boundary layer (1.3 and 0.5, respectively, Nezu & Nakagawa 1993; Kaimal & Finnigan 1994; Raupach *et al.* 1996). One measure of the efficiency of vertical momentum transport is the correlation coefficient between horizontal and vertical turbulent fluctuations, defined as

$$r_{uw} = \frac{u_*^2}{u_{rms} w_{rms}} = \frac{(w_{rms}/u_{rms})}{(w_{rms}/u_*)^2}. \tag{3.1}$$

Relative to a boundary layer, the mixing efficiency is 50 % higher in obstructed shear flows.

4. Distinguishing features

In the context of this study, the ideal obstructed shear flow is deep with a long, uniform and comparatively sparse ($n > 0.9$) permeable medium. In such a flow, the free surface does not impact vortex growth, the obstruction height and density are easily defined and the Reynolds number of the interfacial flow is high (allowing reasonable estimates of C_D). While figure 4 demonstrates similarities across the range of obstructed shear flows, each system has peculiarities which distinguish it from the ideal. Such distinguishing features are discussed below.

4.1. *Dense porous media*

In aquatic flows, sediment beds can be sufficiently dense so as to render the interfacial flow laminar. Indeed, the Reynolds number ($Re = U_h(C_D a)^{-1}/\nu$, where ν is fluid viscosity) of each of the nine DPM studies discussed here is less than 1. At such low Reynolds numbers, it is possible that viscosity damps the vortex instability (in contrast, $Re \sim O(100)$ in the numerical simulation in figure 1*d*). Certainly, a quadratic drag law, where C_D is $O(1)$ and independent of Re, will not strictly apply. Figure 4(*a*) shows that the penetration of shear into DPM (often referred to as the Brinkman layer thickness) is $O(1/3a)$. This is also true in the other obstructed shear flows studied here, for which $C_D \sim O(1)$.

The idea of a diffusive boundary layer above sediment beds, where diffusion occurs at molecular rates (e.g. Lorke *et al.* 2003), is common and can be practically applied to predict solute fluxes from the sediment. This analysis does not prove the existence of coherent vortices at the sediment–water interface. However, in combination with the modelling work of Breugem *et al.* (2006) (figure 1*d*), it does put forth the possibility that the concept of a diffusive boundary layer might be flawed in some cases (particularly for highly porous beds at high Reynolds number). That is, interfacial mixing may in fact be governed by coherent structures rather than by Brownian motion. Importantly, the velocity profiles of all DPM studied here (which have

porosities as low as 0.4) contain the necessary inflection point. Furthermore, linear stability analysis suggests that flow over a permeable medium will be unstable (in the absence of viscosity) for all non-zero porosities (White & Nepf 2007). However, the lack of DPM data points in figure 4(*b–d*), along with an inability to accurately quantify C_D for DPM, prevents further analysis. It is interesting to note that the results of direct numerical simulation of flow over a highly porous packed bed (Breugem *et al.* 2006, $n = 0.95$) agree very well with figure 4. Using peak values of r.m.s. velocities, the coefficients in the relationships in figure 4(*b–d*) are 2.7, 1.1 and 0.6 (respectively) in that flow. However, the impact of porosity on (*a*) the potential for viscous damping of the instability and (*b*) the drag coefficient of a DPM is not well understood. Indeed, the structure of interfacial turbulence in flows over DPM requires a greater research focus.

4.2. *Vegetation canopies*

As mentioned, vegetation canopies (both aquatic and terrestrial) can have significant flexibility and exhibit the dynamically important *ho-/monami*. While the waving canopy data (brown triangles) follow the general trends in figure 4, it is difficult to determine or predict key characteristics, such as C_D or h, of a canopy whose geometry oscillates over time. Also, due to light requirements, submerged aquatic vegetation is typically found in shallow regions (Chambers & Kalff 1985; Duarte 1991), where the free surface may restrict vortex development (Nepf & Vivoni 2000).

4.3. *Urban canopies*

Urban canopies are rarely uniform, with building height and spacing varying significantly. Uniform patches of buildings may be much smaller than L_T, which would be $O(100\ \mathrm{m})$ for a typical urban canopy (Ghisalberti & Nepf 2009). This would result in a flow with diminished vortex penetration, relative to the trend line in figure 4(*a*). Indeed, the two urban canopy data points in this figure (black triangles) fall below the general trend.

While each system has unique features, the common inflectional velocity profile creates an inherent similarity among obstructed shear flows.

The author would like to thank Greg Ivey and Brett Branco for their insight and feedback during the preparation of this manuscript.

REFERENCES

Agelinchaab, M., Tachie, M. F. & Ruth, D. W. 2006 Velocity measurement of flow through a model three-dimensional porous medium. *Phys. Fluids* **18**, 017105.

Amiro, B. D. 1990*a* Comparison of turbulence statistics within three boreal forest canopies. *Bound.-Layer Meteorol.* **51**, 99–121.

Amiro, B. D. 1990*b* Drag coefficients and turbulence spectra within three boreal forest canopies. *Bound.-Layer Meteorol.* **52**, 227–246.

Baldocchi, D. D. & Meyers, T. P. 1988 Turbulence structure in a deciduous forest. *Bound.-Layer Meteorol.* **43**, 345–364.

Breugem, W. P., Boersma, B. J. & Uittenbogaard, R. E. 2006 The influence of wall permeability on turbulent channel flow. *J. Fluid Mech.* **562**, 35–72.

Brunet, Y., Finnigan, J. J. & Raupach, M. R. 1994 A wind tunnel study of air flow in waving wheat: single-point velocity statistics. *Bound.-Layer Meteorol.* **70**, 95–132.

Chambers, P. A. & Kalff, J. 1985 Depth distribution and biomass of submersed aquatic macrophyte communities in relation to Secchi depth. *Can. J . Fish. Aquat. Sci.* **42**, 701–709.

Cheng, H. & Castro, I. P. 2002 Near wall flow over urban-like roughness. *Bound.-Layer Meteorol.* **104**, 229–259.

Chu, V. H. & Babarutsi, S. 1988 Confinement and bed-friction effects in shallow turbulent mixing layers. *J. Hydraul. Engng* **114** (10), 1257–1274.

Coceal, O. & Belcher, S. E. 2004 A canopy model of mean winds through urban areas. *Quart. J. R. Meteorol. Soc.* **130**, 1349–1372.

Duarte, C. M. 1991 Seagrass depth limits. *Aquat. Bot.* **40**, 363–377.

Dunn, C., Lopez, F. & Garcia, M. 1996 Mean flow and turbulence in a laboratory channel with simulated vegetation. *Hydraul. Eng. Ser. 51*, UILU-ENG-96-2009, Department of Civil Engineering, University of Illinois at Urbana-Champaign, Urbana, IL.

Finnigan, J. 2000 Turbulence in plant canopies. *Annu. Rev. Fluid Mech.* **32** (1), 519–571.

Gao, W., Shaw, R. H. & Paw U, K. T. 1989 Observation of organized structure in turbulent flow within and above a forest canopy. *Bound.-Layer Meteorol.* **47**, 349–377.

Gardiner, B. A. 1994 Wind and wind forces in a plantation spruce forest. *Bound.-Layer Meteorol.* **67**, 161–186.

Ghisalberti, M. & Nepf, H. M. 2002 Mixing layers and coherent structures in vegetated aquatic flows. *J. Geophys. Res.* **107** (C2), 3-1–3-11.

Ghisalberti, M. & Nepf, H. M. 2004 The limited growth of vegetated shear layers. *Water Resour. Res.* **40**, W07502.

Ghisalberti, M. & Nepf, H. 2005 Mass transport in vegetated shear flows. *Environ. Fluid Mech.* **5** (6), 527–551.

Ghisalberti, M. & Nepf, H. 2006 The structure of the shear layer in flows over rigid and flexible canopies. *Environ. Fluid Mech.* **6**, 277–301.

Ghisalberti, M. & Nepf, H. 2009 Shallow flows over a permeable medium: the hydrodynamics of submerged aquatic canopies. *Transp. Porous Med.* **78** (3), 385–402.

Goharzadeh, A., Khalili, A. & Jørgensen, B. B. 2005 Transition layer thickness at a fluid-porous interface. *Phys. Fluids* **17,** 057102.

Gupte, S. K. & Advani, S. G. 1997 Flow near the permeable boundary of an aligned fibre preform: an experimental investigation using laser doppler anemometry. *Polym. Compos.* **18** (1), 114–124.

Ikeda, S. & Kanazawa, M. 1996 Three-dimensional organized vortices above flexible water plants. *J. Hydraul. Engng – ASCE* **122** (11), 634–640.

Kaimal, J. C. & Finnigan, J. J. 1994 *Atmospheric Boundary Layer Flows: Their Structure and Measurement*. Oxford University Press.

Kastner-Klein, P. & Rotach, M. W. 2004 Mean flow and turbulence characteristics in an urban roughness sublayer. *Bound.-Layer Meteorol.* **111**, 55–84.

Katul, G. G. & Albertson, J. D. 1998 An investigation of higher-order closure models for a forested canopy. *Bound.-Layer Meteorol.* **89**, 47–74.

Kruijt, B., Malhi, Y., Lloyd, J., Nobre, A. D., Miranda, A. C., Pereira, M. G. P., Culf, A. & Grace, J. 2000 Turbulence statistics above and within two Amazon rain forest canopies. *Bound.-Layer Meteorol.* **94**, 297–331.

Kundu, P. K. & Cohen, I. M. 2004 *Fluid Mechanics*, 3rd edn. Elsevier Academic Press.

Lorke, A., Müller, B., Maerki, M. & Wüest, A. 2003 Breathing sediments: the control of diffusive transport across the sediment–water interface by periodic boundary-layer turbulence. *Limnol. Oceanogr.* **48** (6), 2077–2085.

Louka, P., Belcher, S. E. & Harrison, R. G. 2000 Coupling between air flow in streets and the well-developed boundary layer aloft. *Atmos. Environ.* **34**, 2613–2621.

Lowe, R. 2005 The effect of surface waves on mass and momentum transfer processes in shallow coral reef systems. PhD thesis, Department of Civil and Environmental Engineering, Stanford University.

Lowe, R. J., Koseff, J. R. & Monismith, S. G. 2005 Oscillatory flow through submerged canopies: 1. Velocity structure. *J. Geophys. Res.* **110**.

Macdonald, R. W. 2000 Modelling the mean velocity profile in the urban canopy layer. *Bound.-Layer Meteorol.* **97**, 25–45.

Murphy, E., Ghisalberti, M. & Nepf, H. 2007 Model and laboratory study of dispersion in flows with submerged vegetation. *Water Resour. Res.* **43**, W05438.

Nepf, H., Ghisalberti, M., White, B. & Murphy, E. 2007 Retention time and dispersion associated with submerged aquatic canopies. *Water Resour. Res.* **43**, W04422.

Nepf, H. M. & Vivoni, E. R. 2000 Flow structure in depth-limited, vegetated flow. *J. Geophys. Res.* **105** (C12), 28547–28557.

Nezu, I. & Nakagawa, H. 1993 *Turbulence in Open-Channel Flows*. Balkema.

Novak, M. D., Warland, J. S., Orchansky, A. L., Ketler, R. & Green, S. 2000 Wind tunnel and field measurements of turbulent flow in forests. Part I: uniformly thinned stands. *Bound.-Layer Meteorol.* **95**, 457–495.

Oikawa, S. & Meng, Y. 1995 Turbulence characteristics and organized motion in a suburban roughness sublayer. *Bound.-Layer Meteorol.* **74**, 289–312.

Pasche, E. & Rouvé, G. 1985 Overbank flow with vegetatively roughened flood plains. *J. Hydraul. Engng – ASCE* **111** (9), 1262–1278.

Poggi, D., Porporato, A., Ridolfi, L., Albertson, J. D. & Katul, G. G. 2004 The effect of vegetation density on canopy sublayer turbulence. *Bound.-Layer Meteorol.* **111**, 565–587.

Raupach, M. R., Coppin, P. A. & Legg, B. J. 1986 Experiments on scalar dispersion within a model plant canopy. Part I: the turbulence structure. *Bound.-Layer Meteorol.* **35**, 21–52.

Raupach, M. R., Finnigan, J. J. & Brunet, Y. 1996 Coherent eddies and turbulence in vegetation canopies: the mixing-layer analogy. *Bound.-Layer Meteorol.* **78**, 351–382.

Reidenbach, M. A., Koseff, J. R. & Koehl, M. A. R. 2009 Hydrodynamic forces on larvae affect their settlement on coral reefs in turbulent, wave-driven flow. *Limnol. Oceanogr.* **54** (1), 318–330.

Reidenbach, M. A., Koseff, J. R. & Monismith, S. G. 2007 Laboratory experiments of fine-scale mixing and mass transport within a coral canopy. *Phys. Fluids* **19**, 075107.

Rotach, M. W., Vogt, R., Bernhofer, C., Batchvarova, E., Christen, A., Clappier, A., Feddersen, B., Gryning, S.-E., Martucci, G., Mayer, H., Mitev, V., Oke, T. R., Parlow, E., Richner, H., Roth, M., Roulet, Y.-A., Ruffieux, D., Salmond, J. A., Schatzmann, M. & Voogt, J. A. 2005 BUBBLE – an urban boundary layer meteorology project. *Theor. Appl. Climatol.* **81**, 231–261.

Seginer, I., Mulhearn, P. J., Bradley, E. F. & Finnigan, J. J. 1976 Turbulent flow in a model plant canopy. *Bound.-Layer Meteorol.* **10**, 423–453.

Shaw, R. H., den Hartog, G., King, K. M. & Thurtell, G. W. 1974 Measurements of mean wind flow and three-dimensional turbulence intensity with a mature corn canopy. *Agric. Meteorol.* **13**, 419–425.

Su, H.-B., Schmid, H. P., Vogel, C. S. & Curtis, P. S. 2008 Effects of canopy morphology and thermal stability on mean flow and turbulence statistics observed inside a mixed hardwood forest. *Agric. Forest Meteorol.* **148**, 862–882.

White, B. L. & Nepf, H. M. 2007 Shear instability and coherent structures in shallow flow adjacent to a porous layer. *J. Fluid Mech.* **593**, 1–32.

Wilson, J. D., Ward, D. P., Thurtell, G. W. & Kidd, G. E. 1982 Statistics of atmospheric turbulence within and above a corn canopy. *Bound.-Layer Meteorol.* **24**, 495–519.

Yi, C., Monson, R. K., Zhai, Z., Anderson, D. E., Lamb, B., Allwine, G., Turnipseed, A. A. & Burns, S. P. 2005 Modeling and measuring the nocturnal drainage flow in a high-elevation, subalpine forest with complex terrain. *J. Geophys. Res.* **110**, D22303.